A numerical optimization approach to acoustic hull array design

Thomas A. Wettergren, John P. Casey, and Roy L. Streit
Naval Undersea Warfare Center, 1176 Howell Street, Newport, Rhode Island 02841

(Received 3 January 2002; revised 13 September 2002; accepted 15 September 2002)

A numerical optimization approach is presented to optimize passive broadband detection performance of hull arrays through the adjustment of array shading weights. The approach is developed for general hull arrays in low signal-to-noise ratio scenarios, and is shown to converge rapidly to optimal solutions that maximize the array's deflection coefficient. The beamformer is not redesigned in this approach; only the shading weights of the conventional beamformer are adjusted. This approach allows array designers to use the array to minimize the impact of known sources of noise on detection at the beamformer output while maintaining acoustic array gain against an unknown source. The technique is illustrated through numerical examples using hull-borne structural noise as the noise source; however, the design concept can be applied to other design parameters of the array such as element position, material selection, etc. © *2002 Acoustical Society of America.* [DOI: 10.1121/1.1518982]

PACS numbers: 43.30.Wi, 43.40.Ph, 43.30.Yj [WMC]

I. INTRODUCTION

Traditional approaches to acoustic hull array design have focused on the optimization of desirable beam properties such as the maximization of array gain or the minimization of sidelobe levels. Passive arrays typically employ data-independent beamforming, where the beamformer weights are chosen *a priori* to approximate a desired response oriented in the steered direction. Beam pattern design for linear and planar array geometries has been studied analytically for decades (see, e.g., the classic papers by Dolph[1] and Taylor[2]), but these approaches base their design on achieving some desirable beam characteristics at a fixed frequency, and they focus on trade-offs between beamwidth and sidelobe structure. Single-frequency approaches (see Ref. 3, for example) only indirectly support the fundamental design goal of a passive acoustic hull array, which is to obtain an optimal broadband detection capability in a specified frequency band. Furthermore, the response of the array to nonacoustic noise cannot be assessed through standard beam pattern design techniques.

Passive broadband detection capability of a hull array is degraded by the presence of structural noise. This noise is often reduced by mechanical means (such as isolating mounts, pressure release materials, etc.). A supplementary means to reduce the impact of structural noise on passive detection is to adjust the beamformer weightings to reduce the impact of this noise while maintaining desirable beam characteristics for incoming acoustic waves. This is accomplished (for Gaussian signals) by numerically maximizing the deflection coefficient of a classical square-law detector under the assumption of a small signal-to-noise ratio (SNR). Under this approach, the underlying detection processor is not altered; rather, the conventional beamformer processor is used and the shading weights are treated as available design parameters to be optimized. The design concept is to predict the noise at the hydrophone outputs and then use this local noise field information to mitigate its effect on broadband array detection processing. The parameters which are adjusted are the beamformer weighting (shading) coefficients, and the optimization finds optimal values that replace any conventionally derived weightings. While the example herein is for shading weight adjustment, the design concept can be applied to other design parameters of the array such as element position, material selection, etc.

A computational approach is feasible since structural noise is highly predictable, and current computer hardware and software capabilities enable the numerical optimization of very large degree-of-freedom systems. In this paper, the improvement of passive hull array detection performance through numerical optimization of shading weights is developed. The underlying formulation of this problem has been discussed in Ref. 4 and the references therein. In Sec. II, the broadband hull array detection problem presents a performance metric which can be optimized through shading weights against an unknown acoustic signal. In Sec. III, this detection problem is formulated as a numerical optimization problem and its solution is discussed. In Sec. IV, the approach is applied to a simple numerical example to demonstrate its utility. The paper concludes with recommendations about the use of the method in hull array design.

II. HULL-MOUNTED BROADBAND SONAR DETECTION

Consider a conformal array of sensors (hydrophones) that is electronically steered to receive an incoming acoustic plane wave in the look direction given by the unit vector $\boldsymbol{\xi}_l$. This passive array system is looking for weak signals of unknown spectrum in the presence of noise. The hydrophone array receives noise as well as signal, where the signal is assumed small in received level compared to the noise, and the signal and noise are statistically independent. In this context, noise refers to all contributions to hydrophone response other than the desired acoustic plane wave, so that noise includes ambient noise, structure-borne noise, electronic noise, and acoustic sources outside of the look direction. The hydrophone array is beamformed using a standard broadband

delay-and-sum beamformer, and a square-law postbeamforming detection processing scheme is used.

The detection performance of the passive broadband array is measured by the deflection coefficient. In standard hypothesis testing, the deflection coefficient d for distinguishing signal-plus-noise from noise alone, where both hypotheses are governed by Gaussian random variables, is given by[5]

$$d=\frac{\mu_{SN}-\mu_N}{\sigma_N}, \tag{2.1}$$

if the two hypotheses have the same variance, as is the case of low SNR. We use μ and σ to denote the mean and standard deviation, and subscripts S and N to represent the signal-only and noise-only hypotheses, respectively, and SN to represent the combined signal-plus-noise hypothesis. In a standard square-law detector scheme, the standard deviation σ_N of the noise-only hypothesis is given by (see Ref. 5 for details)

$$\sigma_N=\left[\frac{1}{\pi T}\int_{-\infty}^{+\infty}|H_0(\omega)|^4V_N^2(\omega)d\omega\right]^{1/2}, \tag{2.2}$$

where T is the system averaging time, $V_N(\omega)$ is the beamformer output power spectrum due to noise only, and $H_0(\omega)$ is the predetection filter transfer function. Expression (2.2) assumes that the averaging time T is large compared to the correlation time of the beamformer output under the noise-only conditions. Since the SNR is small, the standard deviation of the signal-plus-noise hypothesis is the same as (2.2). The mean value of the signal-plus-noise hypothesis is given by

$$\mu_{SN}=\frac{1}{2\pi}\int_{-\infty}^{+\infty}|H_0(\omega)|^2V_{SN}(\omega)d\omega, \tag{2.3}$$

where, due to the statistical independence of signal and noise, $V_{SN}(\omega)=V_S(\omega)+V_N(\omega)$, with $V_S(\omega)$ and $V_N(\omega)$ representing the signal-only and noise-only beamformer output power spectra, respectively, in the given look direction $\boldsymbol{\xi}_l$. The mean difference in Eq. (2.1) is thus given by

$$\begin{aligned}\mu_{SN}-\mu_N&=\frac{1}{2\pi}\int_{-\infty}^{+\infty}|H_0(\omega)|^2(V_{SN}(\omega)-V_N(\omega))d\omega\\&=\frac{1}{2\pi}\int_{-\infty}^{+\infty}|H_0(\omega)|^2V_S(\omega)d\omega.\end{aligned} \tag{2.4}$$

When the source spectrum is completely unknown, the predetection filter $H_0(\omega)$ is typically omitted, in which case the deflection coefficient is given by

$$d=\frac{\frac{1}{2}\sqrt{T/\pi}\int_{-\infty}^{+\infty}V_S(\omega)d\omega}{\left[\int_{-\infty}^{+\infty}V_N^2(\omega)d\omega\right]^{1/2}}. \tag{2.5}$$

This expression is used for the remainder of this paper; if a specific predetection filter is to be used in the system under study, the deflection coefficient is easily modified appropriately.

The beamformer output spectrum is dependent on unknown signal characteristics, so it cannot be improved through a passive array design optimization. However, the beamformer output spectrum $V_N(\omega)$ due to noise alone can be written, in part, in terms of predictable structural noise terms. The noise prediction is accomplished through physics-based models of array structural response, empirical data, or a combination of the two. It is through this predictable contribution that the array design is optimized.

An array of M hydrophones is located along a hull at the positions $\{\mathbf{p}_m\}_{m=1}^M$. The beamformer output in the look direction $\boldsymbol{\xi}_l$ is given by the autocorrelation of the time output beamformed response as

$$V(\omega)=\int_{-\infty}^{+\infty}E[v(t)v(t+\tau)]e^{-i\omega\tau}d\tau, \tag{2.6}$$

where $E[\cdot]$ represents the expected value operation and $v(t)$ is the time-domain beamformer output. The time-domain beamformer output for the M hydrophones with look direction $\boldsymbol{\xi}_l$ is given by

$$v(t)=\sum_{m=1}^{M}w_mu_m(t-(\mathbf{p}_m\cdot\boldsymbol{\xi}_l)/c), \tag{2.7}$$

where c is the sound speed and $u_m(t)$ is the time-domain response of the mth hydrophone. The time-domain array element response $u_m(t)$ is due to either (1) the incident plane wave for the source-only case $V_S(\omega)$ or (2) the combination of noise sources for the noise-only case $V_N(\omega)$.

For omnidirectional hydrophones, the electronically steered array phasing matches that of an incident source plane wave in the look direction, so that

$$V_S(\omega)=S(\omega)\left(\sum_{m=1}^{M}w_m\right)^2, \tag{2.8}$$

where $S(\omega)$ is the power spectrum of the source signal. The hydrophone response to a single noise source on the hull is given by the convolution of the noise source waveform $\alpha(t)$ with the impulse response function $h_m(t)$ of the mth hydrophone relative to a unit impulse force at the noise source location. The impulse response function $h_m(t)$ is well defined because the structural-acoustics problem is modeled as a linear system; thus,

$$u_m(t)=\int_{-\infty}^{+\infty}h_m(\mu)\alpha(t-\mu)d\mu. \tag{2.9}$$

Substituting (2.9) into (2.7), it can be shown that the noise-only beamformer output power spectrum is given by

$$V_N(\omega)=A(\omega)\left|\sum_{m=1}^{M}w_mH_m(\omega)e^{i\omega(\mathbf{p}_m\cdot\boldsymbol{\xi}_l)/c)}\right|^2, \tag{2.10}$$

where

$$A(\omega)=\int_{-\infty}^{+\infty}E[\alpha(t)\alpha(t+\tau)]e^{-i\omega\tau}d\tau \tag{2.11}$$

is the power spectrum of the noise source $\alpha(t)$, and

$$H_m(\omega)=\int_{-\infty}^{+\infty}h_m(\mu)e^{-i\omega\mu}d\mu \tag{2.12}$$

is the spectral transfer function (or spectral Green's function) between the noise source location and the mth hydrophone.

The expression derived above for the array response to a single-point noise source with power spectrum $A(\omega)$ is written in vector-matrix form as

$$V_N(\omega)=\mathbf{X}^*(w,\omega)\mathbf{H}^*(\omega)A(\omega)\mathbf{H}(\omega)\mathbf{X}(w,\omega), \quad (2.13)$$

where $(\cdot)^*$ represents the complex conjugate transpose. In this expression, $\mathbf{H}(\omega)$ is a row vector of the spectral transfer functions $[H_1(\omega),H_2(\omega),\ldots,H_M(\omega)]$ and $\mathbf{X}(w,\omega)$ is the beamformer process (column) vector, which is given by

$$\mathbf{X}(w,\omega)=\begin{bmatrix} w_1\exp(ik_0(\mathbf{p}_1\cdot\boldsymbol{\xi}_l)) \\ \vdots \\ w_M\exp(ik_0(\mathbf{p}_M\cdot\xi_l)) \end{bmatrix}, \quad (2.14)$$

where $k_0=\omega/c$ is the free-space wave number. Since $\mathbf{H}(\omega)$ is a row vector of length M, the term $\mathbf{H}^*(\omega)A(\omega)\mathbf{H}(\omega)$ is an $M\times M$ matrix representing the relative complex responses of the M hydrophones to the noise source.

The analysis for multiple known structural noise sources follows the analysis for the single noise source. For K discrete (possibly correlated) noise sources, the beamformer output spectrum is given by the Fourier transform of the autocorrelation of the linear superposition of the beamformed responses of the individual noise sources. Thus

$$\begin{aligned} V_N(\omega)&=\int_{-\infty}^{+\infty}E\left[\sum_{k=1}^{K}v_k(t)\sum_{j=1}^{K}v_j(t+\tau)\right]e^{-i\omega\tau}d\tau \\ &=\sum_{k=1}^{K}\sum_{j=1}^{K}\int_{-\infty}^{+\infty}E[v_k(t)v_j(t+\tau)]e^{-i\omega\tau}d\tau, \end{aligned} \quad (2.15)$$

where $v_k(t)$ is the time-domain beamformer output for the kth noise source alone. This is equivalent to

$$V_N(\omega)=\mathbf{X}^*(w,\omega)\mathbf{H}^*(\omega)\mathbf{C}(\omega)\mathbf{H}(\omega)\mathbf{X}(w,\omega), \quad (2.16)$$

where $\mathbf{H}(\omega)$ is now the $K\times M$ matrix of transfer functions whose (k, m) component is the transfer function from the kth source to the mth hydrophone, and $\mathbf{C}(\omega)$ is the $K\times K$ matrix of noise source cross correlations such that the (j, k) component of $\mathbf{C}(\omega)$ is given by

$$\mathbf{C}_{jk}(\omega)=\int_{-\infty}^{+\infty}E[\alpha_j(t)\alpha_k(t+\tau)]e^{-i\omega\tau}d\tau, \quad (2.17)$$

where $\alpha_j(t)$ is the time-domain source function for the jth source.

The matrix $\mathbf{M}(\omega)$, given by

$$\mathbf{M}(\omega)=\mathbf{H}^*(\omega)\mathbf{C}(\omega)\mathbf{H}(\omega), \quad (2.18)$$

is seen to be the cross-correlation matrix of sensor responses due to the combination of noise sources. The beamformer output spectrum for the combined noise sources is thus given by

$$V_N(\omega)=\mathbf{X}^*(w,\omega)\mathbf{M}(\omega)\mathbf{X}(w,\omega). \quad (2.19)$$

It is easy to see that this expression reduces to (2.13) in the case of a single noise source, and furthermore, for uncorrelated noise sources, it reduces to

$$V_N(\omega)=\sum_{j=1}^{K}V_N^{(j)}(\omega), \quad (2.20)$$

where $V_N^{(j)}(\omega)$ is the beamformer output power spectrum for the jth noise source.

The beamformer output spectrum due to noise as shown in (2.16) is a Hermitian form in the array weights w_j. To see this, write $\mathbf{X}(w,\omega)$ as

$$\mathbf{X}(w,\omega)=\mathbf{U}(\omega)\mathbf{W}, \quad (2.21)$$

where

$$\mathbf{W}=[w_1,w_2,\ldots,w_M]^T, \quad (2.22)$$

and

$$\begin{aligned} \mathbf{U}(\omega)=\mathrm{Diag}\{&\exp(ik_0(\mathbf{p}_1\cdot\boldsymbol{\xi}_L)),\exp(ik_0(\mathbf{p}_2\cdot\boldsymbol{\xi}_L)),\ldots, \\ &\exp(ik_0(\mathbf{p}_M\cdot\boldsymbol{\xi}_L))\}. \end{aligned} \quad (2.23)$$

Thus, the general form of the beamformer output power spectrum for the response of a hull array to structural noise is given by

$$V_N(\omega)=\mathbf{W}^T\mathbf{U}^*(\omega)\mathbf{M}(\omega)\mathbf{U}(\omega)\mathbf{W}. \quad (2.24)$$

Under the limit of small SNR assumption, the incident acoustic signal excites only the hydrophones, and not the hull, so the signal and noise responses are uncorrelated and expression (2.5) for the deflection coefficient holds. Then, using the noise-only beamformer output spectrum $V_N(\omega)$ given by (2.24) and the signal-only beamformer output spectrum $V_S(\omega)$ given by (2.8) in the expression for the deflection coefficient d, we arrive at

$$d=\frac{\frac{1}{2}\sqrt{T/\pi}\,(\Sigma_{m=1}^{M}w_m)^2}{[\int_{-\infty}^{+\infty}V_N^2(\omega)d\omega]^{1/2}}\int_{-\infty}^{+\infty}S(\omega)d\omega, \quad (2.25)$$

as the deflection coefficient. The conditions of omnidirectional hydrophones and of negligible acoustic hull excitation are easily removed at the expense of a more complicated mathematical model; however, these more general conditions somewhat obscure the insight obtained from this derivation, and are therefore not presented here.

III. PERFORMANCE OPTIMIZATION

To optimize the broadband detection performance of a passive sonar array, we seek to find a weighting coefficient vector $\mathbf{W}$ [given by Eq. (2.22)] that maximizes the deflection coefficient d over the frequency band of interest, the upper limit of which is denoted by frequency B. We assume appropriate bandpass filters are placed to minimize the out-of-band effects. The effect of these filters is to limit the integrals in (2.25) to the interval $[-B,B]$. By inspection, the deflection coefficient d is invariant to the scale of the weight vector $\mathbf{W}$, so we fix $\Sigma w_m=1$ without loss of generality, thus removing the Σw_m term from expression (2.25) for d.

For a fixed averaging time T and unknown signal $S(\omega)$, the only component of the deflection coefficient that can be optimized at the design stage is the noise-only beamformer output spectrum $V_N(\omega)$. Since the square-root function found in (2.25) is monotonic, it is removed from the optimi-

zation to leave the following objective function which maximizes the deflection coefficient (and hence, the detection performance):

$$J=\int_{-B}^{+B} V_N^2(\omega)\,d\omega$$

$$=\int_{-B}^{+B}[\mathbf{W}^T\mathbf{U}^*(\omega)\mathbf{M}(\omega)\mathbf{U}(\omega)\mathbf{W}]^2 d\omega. \tag{3.1}$$

The available design parameters in this optimization are the beamformer weighting coefficients w_m which enter the objective function J through the vector $\mathbf{W}$. The complete mathematical optimization problem is stated as follows:

$$\min_{w_m} \int_{-B}^{+B} V_N^2(\omega)\,d\omega$$

$$\text{subject to } \sum w_m = 1 \text{ and } w_m \geqslant 0 \text{ for all } m, \tag{3.2}$$

where

$$V_N(\omega)=\mathbf{W}^T\mathbf{U}^*(\omega)\mathbf{M}(\omega)\mathbf{U}(\omega)\mathbf{W}, \tag{3.3}$$

and $\mathbf{W}$ and $\mathbf{U}$ are given by Eqs. (2.22) and (2.23), respectively. Numerical optimization techniques are used to obtain the solution to this optimization problem for each desired look direction $\boldsymbol{\xi}_l$. It is interesting to note that the optimization problem in Eq. (3.2) is equivalent to the adaptive beamforming technique of minimum variance distortionless response (MVDR) in the limit as frequency bandwidth goes to zero.

The objective function (3.1) is the square of a quadratic form of the design parameters $\mathbf{W}$. Locally, this is well approximated by a positive definite quadratic form, so it is expected that sequential quadratic programming (SQP) would be an effective method of numerical optimization. The principle of SQP methods of optimization is to model the optimization problem (objective function plus constraints) by a quadratic subproblem at each step of the optimization process. The solution of the subproblem defines a search direction for the next step of the algorithm. This method has been found by experience to be very effective in a number of application areas, and it is now a standard technique in numerical optimization. SQP methods are known to work well on problems which have smooth nonlinear functions in both the objective and the constraints. The linear constraints in this problem are obviously smooth, and the objective being the integral of a square of a quadratic form is also smooth. Details of the SQP method are found in a number of references, a good survey of the method is in Ref. 6.

Several software packages exist for solving general SQP optimization problems. A discussion of practical numerical issues when implementing SQP methods is found in Ref. 7. For this problem, the package NPSOL[8] from Stanford University's Systems Optimization Laboratory was used, since it performs few evaluations of the objective function, and since each evaluation in our application is a relatively computationally intensive integral over frequency. The performance of the optimization method is measured by tracking the improvement in the objective function at each step. While local convergence (vs global convergence) is an issue with Newton-type optimization methods such as SQP, this is not an issue for this problem because the optimization problem is convex. That is, the objective function J and the constraint functions are convex functions of the unknown weights, which guarantees that any locally optimal solution is a global optimum. (Moreover, in the examples in Sec. IV, numerous starting points are chosen, and it is observed that all arrived at the same optimum.)

For this implementation, the gradient of the objective function is explicitly evaluated as a subroutine call in the software. For the objective function given in Eq. (3.1), the gradient with respect to the unknowns w_m is given by

$$\nabla J=2\int_{-B}^{+B} V_N(\omega)\nabla V_N(\omega)\,d\omega$$

$$=2\int_{-B}^{+B} V_N(\omega)(2\mathbf{U}^*(\omega)\mathbf{M}(\omega)\mathbf{U}(\omega)\mathbf{W})\,d\omega$$

$$=4\left(\int_{-B}^{+B} V_N(\omega)\mathbf{U}^*(\omega)\mathbf{M}(\omega)\mathbf{U}(\omega)\,d\omega\right)\mathbf{W}. \tag{3.4}$$

A useful numerical check on the accuracy of the gradient evaluation is made by verifying the identity

$$\mathbf{W}^T\nabla J=4J. \tag{3.5}$$

This identity is checked at each evaluation. All integrals in the numerical evaluations of the objective function and its gradient are computed using the method of overlapping parabolas as discussed in Ref. 9.

IV. NUMERICAL RESULTS

To illustrate the utility of the beamformer shading optimization technique, consider an 11-element line array that is conformal to the exterior of a spherical steel shell as shown in Fig. 1. The array elements are equally spaced and extend across a 60° arc along the sphere. The shell's thickness-to-radius ratio is 0.01. The interior of the shell is assumed to be air-filled, so that the magnitude of acoustic waves propagating within the cavity is negligible in the context of the structural-acoustics problem, and the shell is immersed in an unbounded water medium. For this example, it is assumed that the array elements provide negligible impact on the shell's response to external forcing. Element to element coupling is also assumed negligible. Thus, the array elements measure the structural acoustic response of the spherical shell to whatever forcing is applied, combined with the acoustic response to an incident acoustic wave. The structural acoustic analysis of such a spherical shell responding to both incident acoustic waves and point forces is well-studied, and results can be found in numerous references, such as Junger and Feit.[10]

Assume the array in Fig. 1 is electronically steered to its main response axis (MRA), which is the direction of the south pole. The array straddles the south pole (the negative z direction). The broadband design frequency for the array under consideration is given by $3 \leqslant ka \leqslant 10$, where k is the

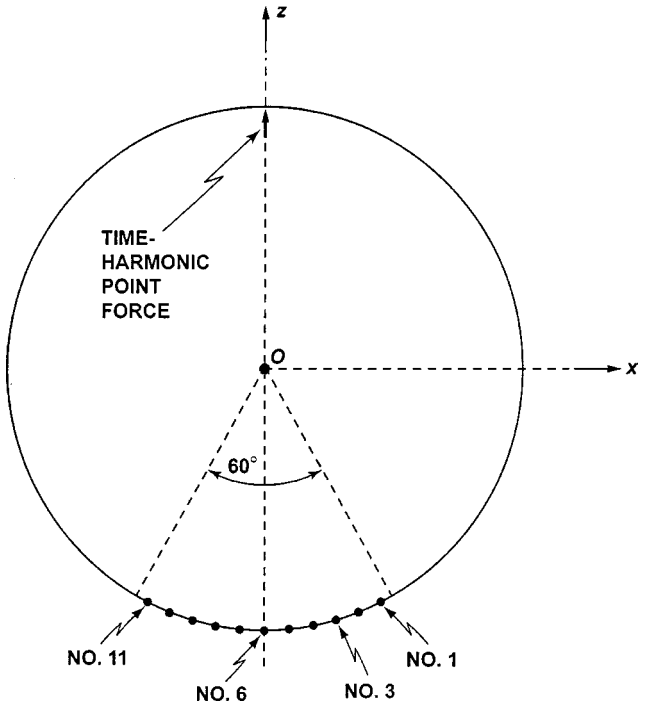

FIG. 1. Array geometry for a spherical shell with conformal 11-element line array.

acoustic wave number in the fluid and a is the shell's exterior radius. At the lower end of this frequency band, the array length is given by $3\lambda/2\pi \approx \lambda/2$, so the low end of the band is the lowest frequency that the array can resolve. The upper frequency is below the Nyquist frequency and large enough to provide a broad sensor frequency band (in this case, the bandwidth is greater than 100% of the center frequency).

An external broadband point force is applied at the north pole of the array, as illustrated in Fig. 1. The spectral content of this force is assumed white over the sensor design frequency band. By computing the array element responses to this force over the entire design frequency band (at 2000 evenly spaced frequency samples), the sensor noise cross-correlation matrix $\mathbf{M}(\omega)$, given by Eq. (2.18), is evaluated. The evaluation of the transfer function in (2.18) is performed using expressions from Junger and Feit.[10] The components of this matrix are functions of frequency, and the (1,1) and (1,2) components are shown in Fig. 2. Note that the (1,1) component is the autocorrelation of the response of element 1 to the broadband point noise source, and the (1,2) component is the cross correlation of elements 1 and 2. The large variations in the structural response over this frequency band show that it is sufficiently broadband that single frequency heuristic designs may do little to improve signal detection performance.

Using the analytical sensor noise cross-correlation matrix in the optimization problem (3.2), with $\mathbf{U}(\omega)$ defined by electronic steering of the array geometry of Fig. 1 to its MRA at the south pole, an optimization of the beamformer shading weights is performed. The results of the optimization are shown as case A in Fig. 3. The symmetry of the optimized weights is a result of the problem symmetry; that is, the array geometry, electronic steering, and noise source all share the same symmetry about the array center. The

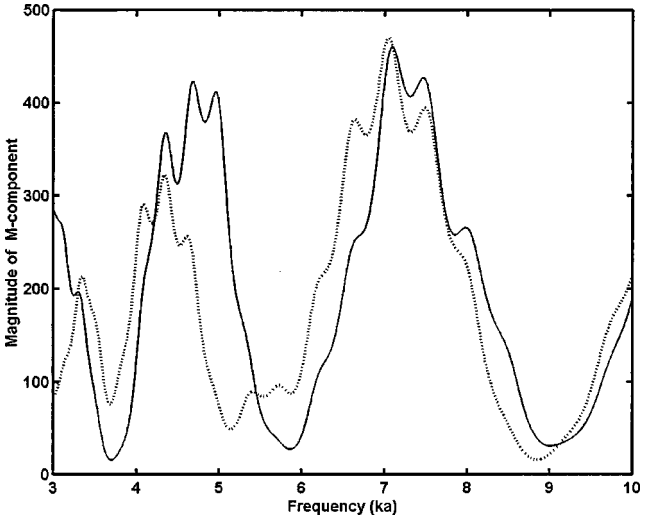

FIG. 2. Cross correlation of sensor responses to the point force: solid line is for sensor 1 correlated with itself, dotted line is for sensor 1 correlated with sensor 2.

"notch" in the center of the array shadings is caused by a large structural vibration response at the middle element of the array over most of the frequency band, which is expected since that element lies at the antipode of the noise forcing function on the thin spherical shell.

To assess the performance of the optimized shading weights, it is illustrative to look at the improvement in deflection coefficient that is achieved by using optimized shading over some nominal shading. The broadband SNR of the beamformer output is proportional to the deflection coefficient d, with the proportionality constant independent of the shading coefficients (given that the noise model includes all sources of noise). By referencing the iterative design improvements to a nominal shading design, the SNR improvement is shown in a manner that is independent of the signal spectrum $S(\omega)$. The SNR improvement of the optimized shading over a uniform shading is given by

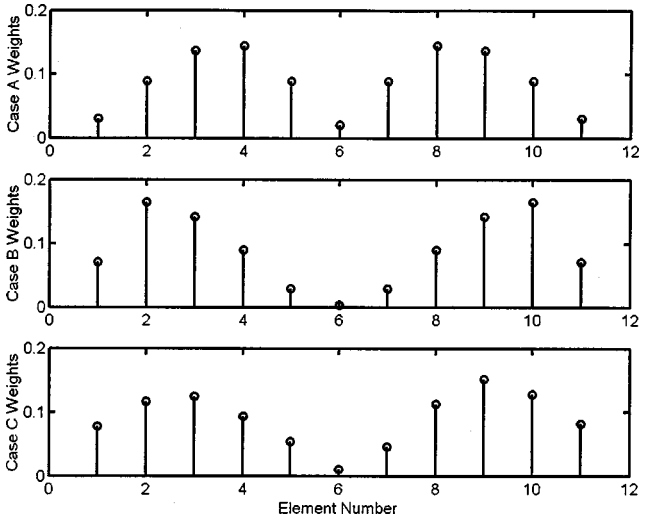

FIG. 3. Optimized weights for 11-element array shown in Fig. 1. Case A is with broadband point noise source steered to MRA. Case B is with broadband equatorial ring noise source steered to MRA. Case C is with broadband point noise source steered to 30° off MRA.

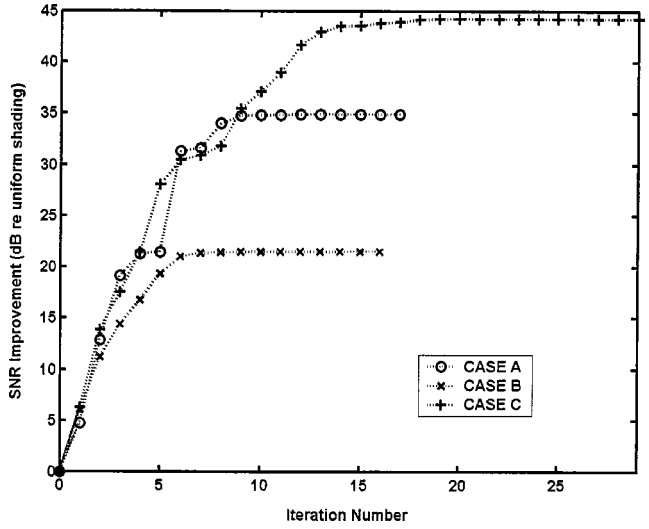

FIG. 4. Convergence of deflection coefficient for optimized results shown in Fig. 3.

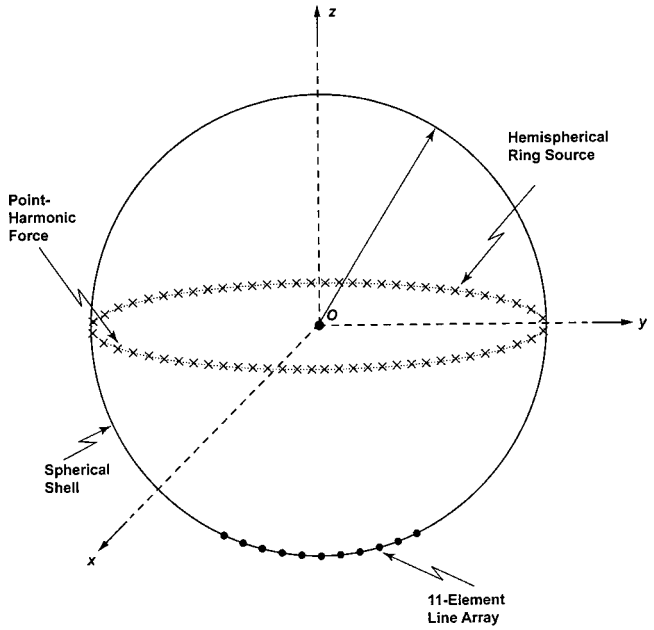

FIG. 5. Array geometry for a spherical shell with equatorial ring force.

$$\text{SNR improvement} = \frac{d(\text{optimum weights})}{d(\text{uniform weights})}. \tag{4.1}$$

For the example of case A, the improvement in SNR of optimal shading weights over uniform shading weights is shown in Fig. 4. In this plot, the improvement in deflection coefficient (relative to uniform shading) is shown as a function of iteration step in the optimization. The improvement starts at 0-dB since the initial condition for the optimization is uniform shading. Numerical experiments were performed with a variety of other initial conditions, but the final optimization results shown are insensitive to the choice of initial condition (as expected because of the problem's convexity).

From Fig. 4, the optimization is seen to converge monotonically, which is expected for a quadratic optimization of a positive definite superquadratic (quartic) objective function. Also note that the convergence is rapid in the early iterations, improving the deflection coefficient by more than 19-dB in just the first three iterations. The surprisingly good results of approximately 35-dB improvement after the convergence of the optimization should be tempered with the realization that the idealized point-driven spherical shell has large resonances that the beamformer shading is able to compensate for by acting as a spatial filter. If the aggregate noise is matched to the noise source model, this improvement translates to 35-dB SNR improvement in detection capability. However, the real situation is mismatched from the single source model in that it has many more components of noise (such as ambient noise, electronics noise, etc.) that combine as in Eq. (2.20) to affect the true deflection coefficient. In practice, it is required that the most dominant of these noise sources be modeled (or measured) and included in the objective function for optimization.

To examine the effect of other types of structural forcing functions, an equatorial ring force was simulated through a series of in-phase broadband point forces distributed along the equator, as shown in Fig. 5. The frequency band of these noise forces was maintained at $3 \leqslant ka \leqslant 10$. The resulting optimized shading weights are shown as case B in Fig. 3 and the convergence of the deflection coefficient over the optimization for case B is shown in Fig. 4. A comparison of these weights with those from the point source show that more of the array center is down weighted, which is expected due to the limited number of modes excited by this force relative to a point force. The more complicated forcing also limits the improvement in deflection performance to only approximately 22-dB. This suggests that adding more noise mechanisms to the model will lower the effectiveness of the optimized array. However, there is still considerable improvement over the nominal case (uniform weights), and the convergence is still monotone. For a specified noise source distribution, any implementation of this method will produce results which are at least as good as the starting values.

The examples of case A and case B were both steered to the array MRA. As an example of the effects of steering, optimization is performed on an array steered to 30° off of the MRA with the point forcing as shown in Fig. 1. The results of this optimization are shown as case C in Figs. 3 and 4. This example shows a slight asymmetry in the weightings, as is expected for a steered array. The resulting performance gain is very large at approximately 44-dB. This large improvement compared to the previous cases is due to the center element of the array sitting at a nodal center of the vibration modes. The center element has a large noise response over most of the band and must be lowered to minimize noise effects. However, minimizing the center element will negatively impact the acoustic reception performance of an array steered to an MRA at the south pole. When the MRA is steered off the south pole, the reception performance is not as severely degraded because of a low center element weighting; thus, total broadband detection performance (deflection coefficient) improves dramatically.

The cases previously shown all consider the bandwidth of the array to be $3 \leqslant ka \leqslant 10$. In Fig. 6, the effect of design

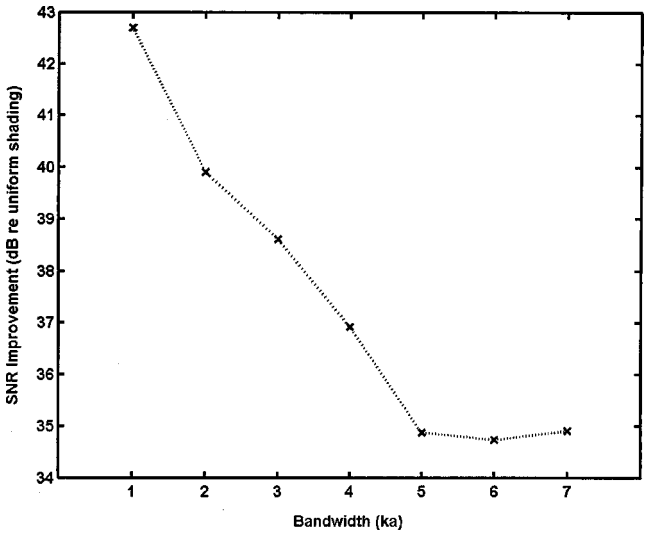

FIG. 6. Optimized deflection coefficient over nominal as a function of bandwidth for the case of the point force with the array steered to MRA.

bandwidth on optimization performance is shown for the case of the point force with the array steered to MRA as the design bandwidth is varied. For this analysis, the frequency range (given by $ka_{\min} \leqslant ka \leqslant ka_{\max}$) is varied with the center frequency held at $ka = 6.5$. As expected, the relative performance improvement due to optimization increases dramatically as the bandwidth is lowered. The performance degradation for increasing bandwidth reaches a plateau near $ka_{\max} - ka_{\min} = 5$. Above this bandwidth, the additional complexity of the additional modes of vibration is beyond the spatial resolution of the 11-element array.

The results shown are very encouraging for practical problems since the optimization produced (a) a constant set of shading weights that reduces the impact of structural noise over the entire broadband frequency range and (b) also maintains enough signal gain to provide improved detection performance over standard designs. To apply the method to arrays that are conformal to large complex structures, the computation of noise transfer functions over the entire broadband frequency range (at as many finely resolved frequency steps as necessary) must be performed. Numerical approaches to efficiently compute these broad frequency sweeps are currently under investigation.

For computational time, the entire 16 iterations of the broadband array shading optimization shown as case A took less than 10 s to run on a 300-MHz workstation. Other cases had similar timing performance. This computation timing assumes that the data matrix $\mathbf{M}(\omega)$ was computed *a priori* and stored as a large text file to be read in at run time. In practical situations, this is accomplished by either running models of all noise sources over the entire band of interest prior to optimization or taking noise data of an actual array and computing $\mathbf{M}(\omega)$ as an average of the measured noise field.

The question of robustness of the numerical optimization with respect to noise uncertainty is not addressed here. The use of a broadband objective function is employed in an attempt to minimize the impact of noise variations on the objective function (3.1). Given the availability of a noise variation model, the extent of the optimal solution's robustness can be measured by forming the Hessian of the objective function (3.1). Such an analysis is a subject of future interest.

V. CONCLUSION

A numerical optimization method is used to optimize passive broadband detection performance of hull arrays through the adjustment of array shading weights. The method is applied to simple examples of a spherical shell with a conformal line array under structural noise. The method shows gains in performance of greater than 20-dB over unity shading for simple noise sources. Convergence of the optimization technique is rapid and guaranteed. The method uses the conventional beamformer framework and optimizes the available design parameters (shading weights). This approach is applicable to any broadband hull array design where problematic noise is known through either measurements or models. Since the approach is to optimize at the design stage, the optimal shading weights obtained can be tabulated for each steering angle in a look-up table in the array beamformer software. Further investigations of the performance of this method with varying types of noise sources (ambient, structural, electronic, etc.) as well as studies of the robustness of the method are planned in the future. While the example shown in this paper is shading weight adjustment, the design concept can be applied to other design parameters of the array such as element position, material selection, etc.

ACKNOWLEDGMENTS

This work was supported by the Naval Undersea Warfare Center's Strategic Initiative program. The authors would like to thank Professor Peter Stepanishen of the University of Rhode Island for pointing out the formulation of the expressions for structural acoustic response of the spherical shell that are found in Junger and Feit.[10]

[1] C. L. Dolph, "A current distribution for broadside arrays which optimizes the relationship between beam width and sidelobe level," Proc. IRE **34**, 335–348 (1946).
[2] T. T. Taylor, "Design of line-source antennas for narrow beamwidth and low side lobes," IRE Trans. Antennas Propag. **AP-1**, 17–20 (1955).
[3] B. D. Van Veen and K. M. Buckley, "Beamforming: A versatile approach to spatial filtering," IEEE ASSP Mag. **5**, 4–24 (1988).
[4] J. P. Casey, and D. Wu, "Numerical acoustic hull array optimization," NUWC-NPT Technical Report 11239, Naval Undersea Warfare Center Division, Newport, RI (2000).
[5] H. L. Van Trees, *Detection, Estimation, and Modulation Theory* (Wiley, New York, 1968), Part I, Chap. 2.
[6] P. T. Boggs and J. W. Tolle, "Sequential quadratic programming," Acta Numerica **4**, 1–51 (1996).
[7] J. Nocedal and S. J. Wright, *Numerical Optimization* (Springer, New York, 1999), Chap. 18.
[8] P. E. Gill, W. Murray, M. A. Saunders, and M. H. Wright, "User's guide for NPSOL 5.0: A FORTRAN package for nonlinear programming," Report SOL 86-1, Dept. of Operations Research, Stanford University (1998), available online at ⟨http://www.stanford.edu/group/SOL⟩.
[9] P. J. Davis and P. Rabinowitz, *Methods of Numerical Integration* (Academic, New York, 1975), Sec. 2.3.
[10] M. C. Junger and D. Feit, *Sound, Structures, and Their Interaction* (MIT Press, Cambridge, MA, 1986), Secs. 7.17–7.19.